JCTC Journal of Chemical Theory and Computation

Least-Action Tunneling Transmission Coefficient for Polyatomic Reactions

Rubén Meana-Pañeda,[†] Donald G. Truhlar,[‡] and Antonio Fernández-Ramos*[,†]

Department of Physical Chemistry, Faculty of Chemistry, University of Santiago de Compostela, 15782 Santiago de Compostela, Spain, and Department of Chemistry and Supercomputing Institute, University of Minnesota, 207 Pleasant Street S. E., Minneapolis, Minnesota 55455-0431

Received August 11, 2009

Abstract: We present a new least-action variational approximation for tunneling in polyatomic reactions based on the procedure developed by Garrett and Truhlar for atom−diatom reactions.[63] The method calculates the semiclassical ground-state tunneling probability at every tunneling energy by minimizing the value of imaginary action integral along a family of paths ranging from the minimum energy path to the straight path. The method is illustrated by applications to two hydrogen-atom abstraction reactions from methane using analytical potential energy surfaces.

1. Introduction

Tunneling is a quantum mechanical effect by which a particle can penetrate into classically forbidden regions of coordinate space.[1−3] Less than 10 years after the formulation of modern quantum mechanics, Wigner[4] and Bell[5] pointed out the importance of this effect in chemical kinetics. Tunneling is very sensitive to the mass of the particles involved in the tunneling motion and to the shape and height of the effective barrier being crossed. Tunneling often competes well with overbarrier processes at low temperatures for processes that involve the transfer of a proton or deuteron. It is well established that quantum tunneling effects require a multidimensional treatment and that they are important processes even at room temperature.[6−9] Because the likelihood of tunneling depends on the mass that is being transferred, the analysis of kinetic isotope effects is one of the chief means of getting insight into the reaction mechanisms of many processes of biological and technological importance.[10,11] Therefore, the treatment of quantum tunneling within a multidimensional framework is very important.

Variational transition-state theory with multidimensional tunneling contributions[12,13] (VTST/MT) has been shown to be capable of accounting for quantum effects on large systems[14,15] but the methodology for treating those effects still allows for some improvements. Here, we present a new approximation that leads to a more complete treatment of quantum tunneling effects in polyatomic chemical reactions.

In section 2, we present background necessary to understand the new work in the context of VTST/MT. Section 3 presents the new LAG4 approximation. Section 4 presents the application of the LAG4 method to the $H + CH_4 \rightarrow H_2 + CH_3$ and $^{15}H + CH_4 \rightarrow {}^{15}H - H + CH_3$ reactions using the Jordan and Gilbert (JG) potential energy surface.[16] Section 5 has concluding remarks.

2. Background

Variational transition-state theory (VTST)[12,13,17−26] is based on transition-state theory (TST), also called conventional transition-state theory, which was originally formulated by Eyring[27] and Evans and Polanyi.[28] TST calculates the one-way equilibrium flux through the transition state (a surface dividing reactants from products in phase space) and assumes that the transition state is a reaction bottleneck that separates reactants from products such that all trajectories that start in the reactants' region and cross the transition state do not recross it before becoming equilibrated as products; this is known as the no recrossing assumption. Furthermore, TST assumes that the Born−Oppenheimer approximation is valid and that the reactants are equilibrated canonically (in a fixed-temperature ensemble) or microcanonically (in a fixed-total-energy ensemble).

* Corresponding author. E-mail: qf.ramos@usc.es.
[†] University of Santiago de Compostela.
[‡] University of Minnesota.

10.1021/ct900420e
Published on Web 11/11/2009

TST and VTST can be formulated unambiguously in a classical world,[29] and quantum effects on all degrees of freedom except the reaction coordinate can reasonably be included by quantizing their partition functions,[27] as justified to order $\hbar^2$ by Wigner.[4] Quantum effects on the reaction coordinate can be incorporated by the addition of a multiplicative multidimensional factor, called the tunneling transmission coefficient,[30−32] but this can only be accomplished consistently in VTST.[33] In fact, VTST/MT incorporates both recrossing (with respect to conventional TST) and quantum tunneling effects, although it needs more information than TST about the potential energy surface of the reaction. TST (without tunneling) needs information only about reactants and the transition state, whereas VTST/MT needs information at least about the reaction path that joins the transition state with reactants and products and sometimes also about a wider region called the reaction swath, which includes additional geometries on the concave side of the reaction path. In the present work, the reaction path is chosen as the minimum energy path (MEP) in isoinertial coordinates,[31,34] scaled to a reduced mass of μ, and the signed distance along this path is labeled as s. By convention, $s = 0$ indicates the location of the transition state, whereas $s < 0$ and $s > 0$ correspond to the reactant and product sides, respectively. The variational method that minimizes the one-way flux from reactants to products through trial dividing surfaces that cross the reaction path at various values of s in a fixed-temperature ensemble is called canonical variational transition-state theory or canonical variational theory (CVT).[20,35] The CVT rate constant for a bimolecular reaction at temperature T is given by

$$k^{\mathrm{CVT}} = \sigma \frac{k_{\mathrm{B}}T}{h} \frac{Q^{\mathrm{GT}}(T, s_*^{\mathrm{CVT}}(T))}{\Phi_{\mathrm{R}}(T)} \exp\left[-V_{\mathrm{MEP}}(s_*^{\mathrm{CVT}}(T))/k_{\mathrm{B}}T\right] \tag{1}$$

where σ is the symmetry number,[36,37] k_{B} and h are the Boltzmann and Planck constants respectively and $V_{\mathrm{MEP}}(s_*^{\mathrm{CVT}}(T))$ is the value of the potential on the reaction path at s_*^{CVT}, which is the location along the reaction coordinate of the dividing surface that minimizes the one-way flux rate constant. The quantized reactant partition function per unit volume is $\Phi_{\mathrm{R}}(T)$, and $Q^{\mathrm{GT}}(T, s_*^{\mathrm{CVT}}(T))$ is the quantized generalized transition-state partition function at $s_*^{\mathrm{CVT}}(T)$.

In this article, we are concerned with quantum effects on the reaction coordinate, which are incorporated by multiplying the CVT rate constant by a transmission coefficient, κ. The resulting rate constant is given by

$$k^{\mathrm{CVT/SAG}}(T) = \kappa^{\mathrm{CVT/SAG}}(T) k^{\mathrm{CVT}}(T) \tag{2}$$

where SAG denotes semiclassical (vibrationally) adiabatic ground state. Neglecting κ is called the quasiclassical approximation.[15] The transmission coefficient, which rigorously is the ratio of the averaged quantum mechanical reaction probabilities to the model underlying TST or VTST without the transmission coefficient, is approximated by the ratio of the averaged SAG and quasiclassical probabilities. The SAG transmission coefficient is evaluated by using an effective potential that (in the first approximation under discussion here) is vibrationally adiabatic with the further approximation[21] that the vibrationally adiabatic potential curves of all of the vibrational excited states have the same shape as the ground-state vibrationally adiabatic potential curve, $V_{\mathrm{a}}^{\mathrm{G}}(s)$, so that all of the tunneling probabilities are evaluated with this potential, which is given in the harmonic approximation by

$$V_{\mathrm{a}}^{\mathrm{G}}(s) = V_{\mathrm{MEP}}(s) + \frac{\hbar}{2} \sum_m \omega_m(s) \tag{3}$$

where $\omega_m(s)$ is a frequency of one of the $3N$-7 ($3N$-6 for linear molecules) generalized normal modes at s. In general, the harmonic approximation used in the evaluation of the vibrationally adiabatic potential is reasonable for polyatomic systems, a major exception being those systems presenting low-frequency internal rotations, for which it is important to include anharmonicity on those torsional modes.[38,39] (Low-frequency modes that are not torsions are also usually anharmonic.) Because the barrier height, $V_{\mathrm{a}}^{\mathrm{AG}}$, of the ground-state vibrationally adiabatic potential curve may be different from $V_{\mathrm{a}}^{\mathrm{G}}(s_*^{\mathrm{CVT}}(T))$, the CVT/SAG transmission coefficient on the right-hand side of eq 2 is equal to an intrinsic transmission coefficient κ^{SAG} times the factor $\exp\{\beta[V_{\mathrm{a}}^{\mathrm{G}}(s_*^{\mathrm{CVT}}(\mathrm{T})) - V_{\mathrm{a}}^{\mathrm{AG}}]\}$ to make the transmission coefficient consistent in spite of the difference in the effective thresholds of the transmission coefficient and of the CVT rate constant. The intrinsic transmission coefficient is given by

$$\kappa^{\mathrm{SAG}}(T) = \frac{\int_0^\infty \mathrm{d}E P^{\mathrm{SAG}}(E) \exp(-\beta E)}{\int_{V_{\mathrm{a}}^{\mathrm{AG}}}^\infty \mathrm{d}E P^{\mathrm{C}}(E) \exp(-\beta E)} \tag{4}$$

where $P^{\mathrm{C}}(E)$ is the classical probability, which equals zero below $V_{\mathrm{a}}^{\mathrm{AG}}$ and unity otherwise, so the transmission factor can be written as:

$$\kappa^{\mathrm{SAG}}(T) = \beta \exp(\beta V_{\mathrm{a}}^{\mathrm{AG}}) \int_0^\infty \mathrm{d}E P^{\mathrm{SAG}}(E) \exp(-\beta E) \tag{5}$$

The semiclassical adiabatic reaction probability of the ground state $P^{\mathrm{SAG}}(E)$ for the whole range of energies is given by

$$P^{\mathrm{SAG}}(E) = \begin{cases} 0, & E < E_0 \\ \{1 + \exp[2\theta(\mathrm{E})]\}^{-1}, & E_0 \le E \le V_{\mathrm{a}}^{\mathrm{AG}} \\ 1 - P^{\mathrm{SAG}}(2V_{\mathrm{a}}^{\mathrm{AG}} - E), & V_{\mathrm{a}}^{\mathrm{AG}} \le E \le 2V_{\mathrm{a}}^{\mathrm{AG}} - E_0 \\ 1, & 2V_{\mathrm{a}}^{\mathrm{AG}} - E_0 < E \end{cases} \tag{6}$$

where E_0 is the lowest energy at which it is possible to have tunneling (this is the energy of the reactant zero-point level when the reaction is written in the exoergic direction) and $\theta(E)$ is the so-called action integral, actually the magnitude of the imaginary part of the action integral:

$$\theta(E) = \hbar^{-1} \int_{\tilde{s}_0}^{\tilde{s}_1} \mathrm{d}s \{2\mu_{\mathrm{eff}}(s)(V_{\mathrm{a}}^{\mathrm{G}}(s) - E)\}^{1/2} \tag{7}$$

where $\mu_{\mathrm{eff}}(s)$ is the effective mass of the tunneling motion, and $\tilde{s}_0$ and $\tilde{s}_1$ are the classical turning points at a given

tunneling energy, E, in the reactant and product valleys, respectively. Both turning points have to obey the resonance condition:

$$V_a^G(\tilde{s}_0) = V_a^G(\tilde{s}_1) = E \tag{8}$$

The simplest case for the evaluation of the action integral of eq 7 is when the coupling between the reaction coordinate and the transverse modes is neglected. In that case, the effective mass equals that of the isoinertial coordinate system, that is, $\mu_{eff}(s) = \mu$. This method is known as the zero-curvature tunneling (ZCT) approximation.[31] The ZCT method is not recommended for general use because it often seriously underestimates the tunneling contribution.[40,41] Wyatt[42] and Marcus and Coltrin[43,44] showed that the coupling enters the reaction-path Hamiltonian through the kinetic energy term producing a negative centrifugal effect that shortens the tunneling path by moving it toward the concave side of the reaction path. This is now called corner-cutting tunneling. Marcus and Coltrin derived a corner-cutting approximation to the transmission coefficient for the collinear H + H_2 reaction (for which the curvature of the MEP in isoinertial coordinates is small) by finding for that case a least-action path, that is, the tunneling path that minimizes eq 7, by incorporating the reaction path curvature (the centrifugal effect) into the effective mass. This method was extended to polyatomic systems by making the vibrationally adiabatic approximation for all bound modes of the transition state,[45] by modifying the effective mass to avoid the singularity in the reaction path Hamiltonian due to the breakdown of the natural collision coordinates when the reaction path curvature is large[46,47] and by properly including the simultaneous corner cutting in more than one mode of vibration.[48,49] The resulting method is called the centrifugal-dominant small-curvature semiclassical adiabatic ground-state (CD-SCSAG) approximation or simply the small-curvature tunneling (SCT) approximation.

For systems with large curvature of the isoinertial MEP, such as bimolecular reactions in which the hydrogen atom is transferred between two heavy atoms,[50] tunneling may be dominated by paths that lie very far from the MEP and, therefore, the adiabatic approximation may breakdown. The large-curvature ground-state tunneling (LCT) method[12,13,48,51−56] was designed for such cases. Other straight-path methods[57−59] have been put forward as well. The latest version of the LCT approximation is called LCG4.[13,56] At each tunneling energy, LCT includes a set of tunneling paths that are the straight trajectory between the two classical turning points at that energy plus the set of all lower-energy tunneling paths. To evaluate action integrals along these paths requires not only information in the potential valley around the MEP (the regions close to the MEP, which can be treated within the adiabatic approximation) but also information about the broader reaction swath on the concave-side of the MEP; this region is the locus of deep-tunneling paths that are vibrationally nonadiabatic. In the LCT approximation, tunneling into excited vibrational states of the products in the exoergic direction is also included;[55] tunneling into excited states is also included for thermoneutral reactions.[60] The LCG4 approximation is more accurate than the previous LCG3 approximation because it includes a nonquadratic correction in the nonadiabatic region. In general, the evaluation of the LCG4 transmission coefficients is quite demanding from the computational point of view, so two interpolated large curvature tunneling (ILCT) methods, called ILCT1D[61] and ILCT2D,[62] were proposed. The latter evaluates the LCG4 transmission coefficient with an error (with respect to the uninterpolated calculation) smaller than 1% but it reduces the computer time by more than one order of magnitude.

The SCT and LCT transmission coefficients cover the whole range of reaction-path curvatures, so it seems natural to built a transmission coefficient which, at every tunneling energy, chooses the largest between the SCT and LCT tunneling probabilities, or similarly (essentially equivalently), the smallest between the SCT and LCT imaginary action integrals. This approximation is called microcanonical optimized multidimensional tunneling (μOMT) method.[55] The μOMT tunneling probabilities are, therefore,

$$P^{\mu OMT}(E) = \max_E \begin{cases} P^{SCT}(E) \\ P^{LCT}(E) \end{cases} \tag{9}$$

where $P^{SCT}(E)$ and $P^{LCT}(E)$ are the SCT and LCT probabilities evaluated within the CD-SCSAG and LCG4 approximations, respectively. However, these two approximations are just two particular cases of a more general method in which the tunneling path is variationally optimized by employing a criterion of least imaginary action. This method, which is called least-action ground-state tunneling (LAT) approximation, was developed some years ago for atom−diatom reactions, and it was shown to be superior to the SCT and LCT methods.[63,64] Other LAT methods using a family of paths similar to that described by Garrett and Truhlar[63] have also been developed for polyatomic reactions, although those methods were only used to compute tunneling splittings. For instance, Taketsugu and Kimihiko[65] used a multidimensional LAT method to obtain the least-action integral at a given tunneling energy. Similarly, Tautermann et al.[66] obtained the optimal tunneling path to predict ground-state tunneling splittings in symmetric polyatomic systems. So far though the LAT method has not been applied to evaluate thermal rate constants for polyatomic systems. However, it has been extensively applied to atom−diatom reactions[41] and compared with SCT and LCT approximations. Although all of the LCT calculations were performed using the LCG3 approximation, it was concluded that, for some cases the μOMT method was as accurate as the LAT method, but on average the latter was superior to the former.

The current μOMT method evaluates the large-curvature probabilities with the LCG4 approximation and it performs well for polyatomic reactions. However, it is interesting to know the effect of full optimization of the tunneling paths in a multidimensional framework in polyatomic reactions even when full optimization may be more expensive computationally than the current methods. In this work, we present a new version, which adds the following features to the previous LAT method: (i) it is now developed for polyatomic reactions, and (ii) it uses the same criteria for

the specification of the adiabatic and nonadiabatic regions as the LCG4 method. Therefore, we label this version of the least-action tunneling method as LAG4.

3. Methods

LAG4, like LCG3 and LCG4, is always applied to a reaction in the exoergic or thermoneutral direction with the reactant in its ground vibrational state. The tunneling process may end in the product ground state or in an excited diabatic vibrational state of the product. In general one sums over the probabilities of producing each final state but, in many cases, one needs to consider only ground-state-to-ground-state tunneling, and this section will start with the ground-state-to-ground-state process.

The LAG4 approximation involves the minimization of the imaginary action integrals along a given set of paths, which are between the MEP and the straight path (which is the reference path for all the LCT methods, including the LCG4 approximation). At a given tunneling energy the end points of any particular tunneling path are given by $\tilde{s}_0$ and $\tilde{s}_1$ with the resonance condition given by eq 8. The mass-scaled Cartesian geometries of these two classical turning points that are located on the MEP are $\mathbf{x}(\tilde{s}_0)$ and $\mathbf{x}(\tilde{s}_1)$, respectively. The paths to initiate the search for the least-action are built as a function of a single parameter α, such that $\alpha = 0$ yields the MEP and $\alpha = 1$ yields the straight path. Therefore, $\alpha = 0$ and $\alpha = 1$ correspond to the ZCT and LCT transmission coefficients, respectively. We introduce a progress variable along the path, called $\xi(\alpha)$, which is in the interval $0 \le \xi(\alpha) \le \xi_P(\alpha)$, where $\xi_P(\alpha)$ is the total length of path at a given tunneling energy.

The lengths of the MEP and of the straight path are $\xi_P(0)$ and $\xi_P(1)$ respectively, so all the intermediate paths obey the condition $\xi_P(1) \le \xi_P(\alpha) \le \xi_P(0)$. The variable γ is defined by

$$\gamma = \frac{\xi(\alpha)}{\xi_P(\alpha)} \tag{10}$$

The γ parameter is in the interval [0, 1], being 0 at the reactants classical turning point and 1 at the products classical turning point. This parameter is useful to unify all of the paths with different α values to see how much relative progress there is along each of them. We prefer to use $\xi(\alpha)$ instead because in this case the length of the paths is explicitly used.

The mass-scaled Cartesian geometries for a given value of α, at a point $\xi(\alpha)$ along the path and at a given tunneling energy, are $\mathbf{x}[\alpha, \xi(\alpha), \tilde{s}_0]$. Thus, the mass-scaled Cartesian geometries along the MEP are given by $\mathbf{x}[0, \xi(0), \tilde{s}_0]$, whereas the ones along the straight path are

$$\mathbf{x}[1, \xi(1), \tilde{s}_0] = \mathbf{x}(\tilde{s}_0) + \xi(1)\hat{\boldsymbol{\eta}}[1, \xi(1), \tilde{s}_0] \tag{11}$$

where $\mathbf{x}(\tilde{s}_0) = \mathbf{x}[0, 0, \tilde{s}_0]$. The parameter $\xi(1)$ indicates the progress along the straight path; $\hat{\boldsymbol{\eta}}[1, \xi(1), \tilde{s}_0]$ is the unit vector along the straight path, that is,

$$\hat{\boldsymbol{\eta}}[1, \xi(1), \tilde{s}_0] = \frac{\mathbf{x}(\tilde{s}_1) - \mathbf{x}(\tilde{s}_0)}{\xi_P(1)} \tag{12}$$

where the length of the straight path is $\xi_P(1) = |\mathbf{x}(\tilde{s}_1) - \mathbf{x}(\tilde{s}_0)|$.

The MEP and the straight path are the extreme cases of a family of $\alpha-$dependent paths, which are chosen as

$$\mathbf{x}[\alpha, \xi(\alpha), \tilde{s}_0] = (1 - \alpha)\mathbf{x}[0, \xi(0), \tilde{s}_0] + \alpha\mathbf{x}[1, \xi(1), \tilde{s}_0] \tag{13}$$

where $\mathbf{x}[0, \xi(0), \tilde{s}_0]$ and $\mathbf{x}[1, \xi(1), \tilde{s}_0]$ are the geometries along the MEP and along the straight path respectively with the same progress, that is, $\xi(0)/\xi_P(0) = \xi(1)/\xi_P(1) = \gamma$.

The imaginary action integral for each of these paths is a generalization of the imaginary action integral along the LCT straight path. At every tunneling energy, the paths of eq 13 are built as a function of the α parameter as shown in Figure 1. For small values of α the geometries along the path will be very close to those along the MEP and therefore motion along the entire path is treated as vibrationally adiabatic. For intermediate to large values of α, the path is divided into three regions. Regions I and III, located on the reactants and products sides respectively are treated as vibrationally adiabatic, and region II is vibrationally nonadiabatic.

The vibrationally adiabatic potential is obtained in such a way that the geometry $\mathbf{x}[\alpha, \xi(\alpha), \tilde{s}_0]$ is perpendicular to the gradient at that s value, that is,

$$\{\mathbf{x}[\alpha, \xi(\alpha), \tilde{s}_0] - \mathbf{x}[0, \xi(0), \tilde{s}_0]\}\frac{\mathrm{d}\mathbf{x}[0, \xi(0), \tilde{s}_0]}{\mathrm{d}s} = 0 \tag{14}$$

The above equation may have multiple solutions but we are interested in the solution that makes s a continuous function of $\xi(\alpha)$. There is no guarantee that eq 14 will be met for any geometry along the tunneling path. To find the solution to eq 14 for a geometry $\mathbf{x}[\alpha, \xi(\alpha), \tilde{s}_0]$ starting from region I, a root search procedure is set up starting from the reactants side turning point $\tilde{s}_0$, that is, at $\xi(\alpha) = 0$. The value of s that satisfies eq 14 is $s_I[\alpha, \xi(\alpha), \tilde{s}_0]$. In the same way can be found a value $s_{III}[\alpha, \xi(\alpha), \tilde{s}_0]$ starting from products at the classical turning point $\tilde{s}_1$. If it is not possible to find a geometry along the MEP that satisfies eq 14, it means that there is no projection for that geometry of the tunneling path onto the modes perpendicular to the reaction path in the interval $[\tilde{s}_0, \tilde{s}_1]$. When this happens going from reactants to products, the nonadiabatic region in the reactants side starts at $\xi(\alpha) = \xi_I(\alpha)$, being $\xi_I(\alpha)$ the last value for which $s_I[\alpha, \xi(\alpha), \tilde{s}_0]$ exists. In the same way, the nonadiabatic region in products side starts at $\xi(\alpha) = \xi_{III}(\alpha)$, being $\xi_{III}(\alpha)$ the last value for which $s_{III}[\alpha, \xi(\alpha), \tilde{s}_0]$ exists.

It may occur that $\xi_{III}(\alpha) < \xi_I(\alpha)$, so there is an overlap between the adiabatic regions and the nonadiabatic region does not exist. In this case, the vibrationally adiabatic potential in the interval $[\xi_{III}(\alpha), \xi_I(\alpha)]$ is evaluated as:

$$\min(V_a^G[s_I(0, \xi(0)); \tilde{s}_0], V_a^G[s_{III}(0, \xi(0)); \tilde{s}_0]) \tag{15}$$

Each of the two $s_i(0, \xi(0))$, $i = \mathrm{I}, \mathrm{III}$ values needed for the evaluation of the vibrationally adiabatic potentials $V_a^G[s_i(0, \xi(0)); \tilde{s}_0)]$ is obtained from eq 14.

In the case that $\xi_{III}(\alpha) > \xi_I(\alpha)$, the potential is nonadiabatic in the region II, which has boundaries $\xi_I(\alpha)$ and $\xi_{III}(\alpha)$ with regions I and III, respectively. Therefore, region I corresponds to $0 \le \xi(\alpha) < \xi_I(\alpha)$, region II to

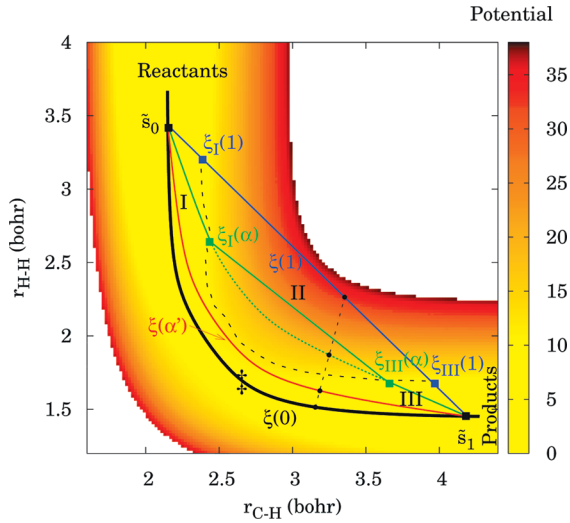

Figure 1. Plot of the JG PES (energy in kcal/mol) as a function of two distances; r_{C-H} is the distance between the carbon atom and the abstracted CH_4 hydrogen atom and r_{H-H} is the distance between the hydrogen atom and the abstracted CH_4 hydrogen atom. The graph also shows some possible reaction paths at a given tunneling energy with classical turning points given by $\tilde{s}_0$ and $\tilde{s}_1$ in the reactant and product sides, respectively. The reaction swath is partitioned into the adiabatic region of reactants (labeled as I), adiabatic region of products (labeled as III), and the nonadiabatic region (labeled as II and with boundaries given by a black dashed line). The symbol ‡ indicates the position of the saddle point, which is the conventional transition state. Four different paths are plotted as solid curves over the PES using eq 13. The four different values of α are 0 (black solid line), 0.10 (red line), 0.50 (green line), and 1 (blue line). The path with $\alpha = 0$ corresponds to the MEP and is labeled as $\xi(0)$. The path with $\alpha = 0.10$ (labeled as $\xi(\alpha')$) corresponds to a curved path passing through a region, which is completely vibrationally adiabatic. The path with $\alpha = 0.50$ (labeled as $\xi(\alpha)$) corresponds to a curved path, which crosses the nonadiabatic region with boundaries given by $\xi_I(\alpha)$ in the reactants side and by $\xi_{III}(\alpha)$ in the products side. In the nonadiabatic region, this path does not follow the curved path (green dotted line) but the straight path (green solid line). Finally, the path with $\alpha = 1$ (labeled as $\xi(1)$) corresponds to the straight path connecting the geometries of the MEP at the classical turning points. The nonadibatic region starts at $\xi_I(1)$ in the reactants side and ends at $\xi_{III}(1)$ in the products side. The black dashed line joining the straight path and the MEP indicates the progress along each of the four tunneling paths for a given value of γ (eq 10).

$\xi_I(\alpha) \le \xi(\alpha) \le \xi_{III}(\alpha)$, and region III to $\xi_{III}(\alpha) < \xi(\alpha) \le \xi_P(\alpha)$. As shown in Figure 1, the path along regions I and III is given by eq 13, whereas the path along region II is a straight path between the boundaries, where the geometries are given by

$$\mathbf{x}[\alpha,\xi(\alpha),\tilde{s}_0] = \mathbf{x}[\alpha,\xi_I(\alpha),\tilde{s}_0] + \frac{\xi(\alpha) - \xi_I(\alpha)}{\xi_{III}(\alpha) - \xi_I(\alpha)}(\mathbf{x}[\alpha,\xi_{III}(\alpha),\tilde{s}_0] - \mathbf{x}[\alpha,\xi_I(\alpha),\tilde{s}_0]) \quad (16)$$

The nonadiabatic region is defined in the same way as for the LCG4 method, that is, the path is in the adiabatic region when (i) the condition given by eq 14 is obeyed, (ii) all the generalized normal mode coordinates are within their vibrational turning points, (iii) the geometry $\mathbf{x}[\alpha, \xi(\alpha), \tilde{s}_0]$ lies within the single-valued region of the reaction path coordinates, and (iv) the adiabatic potential should be greater than or equal to the effective potential at the boundary of the nonadiabatic region; in the other case the nonadiabatic region is extended until this condition is met. On the other hand, if the adiabatic potential is smaller than the effective potential the difference is due to anharmonicity, so the effective potential is modified with a nonquadratic correction.

The imaginary action integral at every tunneling energy and for each α value along the paths of eq 13 is:

$$\theta(\alpha,\tilde{s}_0) = \frac{(2\mu)^{1/2}}{\hbar}\Big[\int_0^{\xi_I(\alpha)} d\xi(\alpha)\{V_a^G[s_I(0,\xi(0);\tilde{s}_0)] - V_a^G(\tilde{s}_0)\}^{1/2} \cos\chi_0\{\tilde{s}_0,\ \hat{\boldsymbol{\eta}}[\alpha,\xi(\alpha),\tilde{s}_0]\} + \int_{\xi_I(\alpha)}^{\xi_{III}(\alpha)} d\xi(\alpha)\{V_{eff}^{II}(\alpha,\xi(\alpha),\tilde{s}_0) - V_a^G(\tilde{s}_0)\}^{1/2} + \int_{\xi_{III}(\alpha)}^{\xi_P(\alpha)} d\xi(\alpha)\{V_a^G[s_{III}(0,\xi(0);\tilde{s}_0)] - V_a^G(\tilde{s}_0)\}^{1/2} \cos\chi_1\{\tilde{s}_1,\ \hat{\boldsymbol{\eta}}[\alpha,\xi(\alpha),\tilde{s}_1]\}\Big] \quad (17)$$

The two cosines of eq 17, $\cos\chi_i\{\tilde{s}_i, \hat{\boldsymbol{\eta}}[\alpha, \xi(\alpha), \tilde{s}_i]\}$ for $i = 0, 1$ are obtained as the dot products between the unit vectors $\hat{\boldsymbol{\eta}}[\alpha, \xi(\alpha), \tilde{s}_i]$ and the unit vectors tangent to the MEP at s_i, that is,

$$\cos\chi_i\{\tilde{s}_i,\hat{\boldsymbol{\eta}}[\alpha,\xi(\alpha),\tilde{s}_i]\} = \hat{\boldsymbol{\eta}}[\alpha,\xi(\alpha),\tilde{s}_i]\frac{d\mathbf{x}(\tilde{s}_i)}{ds}, i = 0,1 \quad (18)$$

The effective potential of eq 17 of the LAG4 method is the same as that of the LCG4 method, with the difference that now the geometries at which the potential is evaluated are functions of α and of the progress variable ξ, which also depends on α. Therefore, the effective potential is given by

$$V_{eff}^{II}(\alpha,\xi(\alpha),\tilde{s}_0) = V\{\mathbf{x}[\alpha,\xi(\alpha),\tilde{s}_0]\} + V_{corr}^{I}(\alpha,\xi_I(\alpha),\tilde{s}_0) + V_{anh}^{I}(\alpha,\tilde{s}_0) + \frac{\xi(\alpha) - \xi_I(\alpha)}{\xi_{III}(\alpha) - \xi_I(\alpha)}[V_{corr}^{III}(\alpha,\xi_{III}(\alpha),\tilde{s}_0) - V_{corr}^{I}(\alpha,\xi_I(\alpha),\tilde{s}_0) + V_{anh}^{III}(\alpha,\tilde{s}_0) - V_{anh}^{I}(\alpha,\tilde{s}_0)] \quad (19)$$

The potentials $V_{corr}^{i}(\alpha, \xi_i(\alpha), \tilde{s}_0)$, $i = I, III$ correct for the zero-point energy in the modes that are still within their turning points. The potentials $V_{anh}^{i}(\alpha, \tilde{s}_0)$ incorporate anharmonic nonquadratic corrections to the effective potential in the same way as in the LCG4 method.

The optimum tunneling path (i.e., the LAG4 path) of the family of paths given by eq 13 is the one that minimizes the imaginary action integral of eq 17. The searching procedure is similar to the one described in ref 12, that is, the smallest value of $\theta(\alpha, \tilde{s}_0)$ is found by a quadratic search in α starting with a initial set of 11 equally spaced points. The optimum value of α at every tunneling energy is labeled as $\tilde{\alpha}$.

The tunneling amplitude of the LAG4 path initiated at $\tilde{s}_0$ is approximated using a primitive semiclassical expression

$$T_{\mathrm{tun}}^{\mathrm{LAG4}}(\tilde{\alpha}, \tilde{s}_0) = T_{\mathrm{tun}}^{\mathrm{LAG4}}(\tilde{\alpha}, \tilde{s}_1) = \exp\left[-\theta(\tilde{\alpha}, \tilde{s}_0)\right] \tag{20}$$

The LAG4 primitive probability, $P_{\mathrm{prim}}^{\mathrm{LAG4}}(E)$, is obtained from the tunneling amplitude of the previous eq 20 plus the contribution due to the vibrational motion perpendicular to the reaction coordinate along the incoming $T_0(E)$ and outgoing $T_1(E)$ trajectories at tunneling energy E

$$P_{\mathrm{prim}}^{\mathrm{LAG4}}(E) = |T_0(E) + T_1(E)|^2 + \left(\frac{\cos\chi_0\{\tilde{s}_0, \hat{\boldsymbol{\eta}}[\tilde{\alpha}, \xi(\tilde{\alpha})\tilde{s}_0]+\}\cos\chi_1\{\tilde{s}_1, \hat{\boldsymbol{\eta}}[\tilde{\alpha}, \xi(\tilde{\alpha}), \tilde{s}_1]\}}{2}\right)^2 \times \exp\left[-2\theta(\tilde{\alpha}, \tilde{s}_0)\right] \tag{21}$$

The tunneling amplitude of the incoming trajectory along the reaction coordinate is $\exp[-\theta(\tilde{\alpha}, \tilde{s}_0)]\times \cos\chi_0\{\tilde{s}_0, \hat{\boldsymbol{\eta}}[\tilde{\alpha}, \xi(\tilde{\alpha}), \tilde{s}_0]\}$ and that of the outgoing trajectory is $\exp[-\theta(\tilde{\alpha}, \tilde{s}_0)]\cos\chi_1\{\tilde{s}_1, \hat{\boldsymbol{\eta}}[\tilde{\alpha}, \xi(\tilde{\alpha}), \tilde{s}_1]\}$. The expression used in eq 21 is the average of the two tunneling amplitudes. Similarly the tunneling amplitude due to the all the vibrational degrees of freedom perpendicular to the reaction coordinate is averaged using $T_0(E)$ and $T_1(E)$, instead of using $2T_0(E)$, to inforce macroscopic reversibility. The expression for $T_0(E)$ is similar to the one given in ref 13 but evaluated along the LAG4 tunneling path ($\alpha = \tilde{\alpha}$) instead of along the LCG4 tunneling path ($\alpha = 1$).

The primitive probability of eq 21 can be greater than one because of the integration of the amplitudes over the incoming and outgoing trajectories, so it is enforced to go to $^1/_2$ at the maximum of the vibrational adiabatic potential $V_{\mathrm{a}}^{\mathrm{AG}}$ by the expression

$$P^{\mathrm{LAG4}}(E) = \left\{1 + \frac{1}{2}\frac{[P_{\mathrm{prim}}^{\mathrm{LAG4}}(V_{\mathrm{a}}^{\mathrm{AG}})^{-1}] - 1}{P_{\mathrm{prim}}^{\mathrm{LAG4}}(V_{\mathrm{a}}^{\mathrm{AG}})} P_{\mathrm{prim}}^{\mathrm{LAG4}}(E)\right\} \times \frac{1}{1 + [P_{\mathrm{prim}}^{\mathrm{LAG4}}(E)]^{-1}} \tag{22}$$

It is possible to include tunneling into excited vibrational states of products in the exoergic direction. It can be done easily by using the LAG4 approximation for the ground state and the LCG4 approximation for excited vibrational states. The procedure is described in detail in ref 13 and will not be discussed here. The LAT method in its LAG4 version has been implemented in *POLYRATE 2008*.[67]

4. Results and Discussion

In this section, we apply VTST/MT, including the LAG4 approximation for the evaluation of the transmission coefficients for two hydrogen abstraction reactions:

$$\mathrm{H} + \mathrm{CH_4} \rightarrow \mathrm{H_2} + \mathrm{CH_3} \tag{R1}$$

$$^{15}\mathrm{H} + \mathrm{CH_4} \rightarrow {}^{15}\mathrm{H} - \mathrm{H} + \mathrm{CH_3} \tag{R2}$$

Both reactions R1 and R2 were studied using the Jordan and Gilbert (JG) potential energy surface (their surface no. 2).[16] In the case of reaction R2, we just have changed the mass of the hydrogen, which is abstracting the proton, to that of a methyl group to observe the effect of the reaction-path curvature on the transmission coefficients. Both reactions are of the type A + BC → AB + C, where A, B, and C are atoms or groups of atoms. The reaction path curvature is a function of the skew angle, which in isoinertial coordinates is given by

$$\beta = \cos^{-1}\left(\frac{m_{\mathrm{A}}m_{\mathrm{C}}}{(m_{\mathrm{A}} + m_{\mathrm{B}})(m_{\mathrm{B}} + m_{\mathrm{C}})}\right)^{1/2} \tag{23}$$

The skew angle is close to 90° when B has a much larger mass than A and C and it is close to zero when the mass of A and C is much larger than the mass of B. For the latter, tunneling effects are more important because a light particle is being transferred between two heavy atoms (heavy-light-heavy system). For reaction R1, the skew angle is $\beta = 47°$, whereas for reaction R2 the skew angle is only $\beta = 20°$. From these values of the skew angle, we expect small values of $\tilde{\alpha}$ at all tunneling energies for reaction R1, because the reaction path curvature is small, whereas large values of $\tilde{\alpha}$ are expected for reaction R2. Indeed, this is the case at low tunneling energies, as shown in Figure 2, which plots the variation of θ with α for every tunneling energy for reactions R1 and R2. For any reaction-path curvature, the least-action path is always the path with the best compromise between length and energy, that is, between short paths with high barriers and long paths with low barriers. The two extreme cases are, on one hand, the straight path, which is the shortest path between two classical turning points but the most unfavorable from the energetic point of view and, on the other hand, the MEP, which is the longest path but the most favorable energetically. The transmission coefficients obtained using these two prescriptions are the LCT, for the straight path, and the ZCT, for the MEP.

For both reactions, at low tunneling energies and for the paths characterized by the optimum $\tilde{\alpha}$, there is an important area of the reaction swath that is vibrationally nonadiabatic and that involves a significant increase of the potential energy. That increase has to be compensated by shortening the length of the path. That compensation occurs for reaction R2, for which the curvature of the reaction path makes the straight path very short, but not for reaction R1, for which decreasing the length of the path does not compensate the increase in potential energy. This is why the incursion of the least-action path into the vibrationally nonadiabatic region is weaker for reaction R1 than for reaction R2. The sudden increase of the action integral observed in Figure 2 for reaction R2 at α values about 0.9 is due to the extension of the nonadiabatic region because for those paths there are geometries for which eq 14 is not satisfied. At high tunneling energies, the whole reaction swath is vibrationally adiabatic and, therefore, there is no rise in energy even for very short paths, so the least-action path coincides with the straight path.

The transmission coefficients and rate constants for reaction R1 are listed in Table 1 and Table 2 respectively, whereas the transmission coefficients for reaction R2 are listed in Table 3. The LAT results for reactions R1 and R2 show that SCT and LAT approximations underestimate the

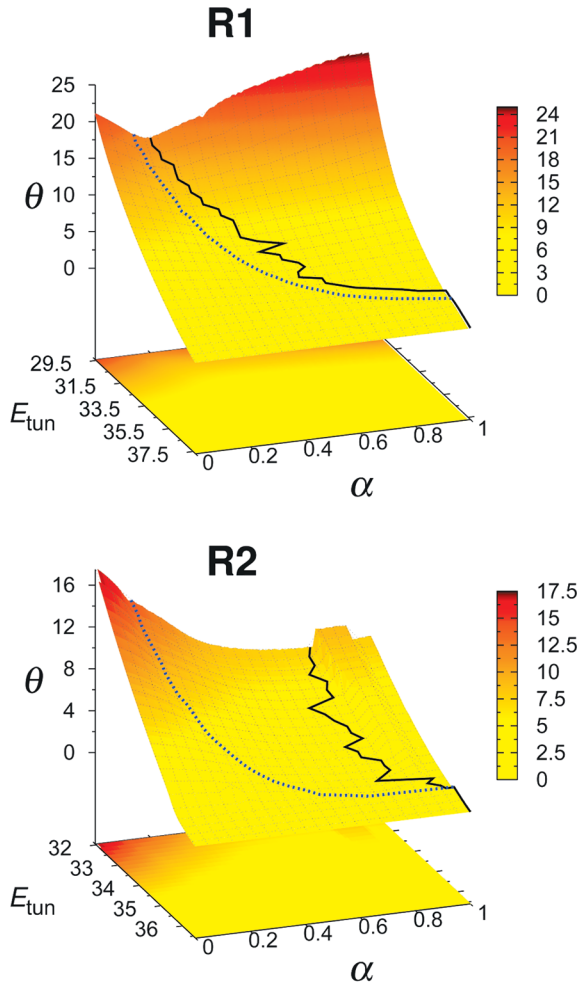

Figure 2. Graphs showing the variation of the imaginary-action integral with the α parameter at each of the tunneling energies (in kcal/mol) for reactions R1 and R2. The solid line indicates the locations of $\tilde{\alpha}$ at every tunneling energy. The dashed line indicates the lowest α value for which there is a nonadiabatic region when the paths given by eq 13 are followed in the direction from reactants to products.

Table 1. Transmission Coefficients for Reaction R1 on the JG Surface

T (K)	ZCT	SCT	LCT	μOMT	LAT
200	4.36	18.7	13.7	18.8	27.3
250	2.49	6.27	5.11	6.28	7.30
300	1.87	3.54	3.04	3.54	3.73
400	1.41	2.02	1.84	2.03	2.01
500	1.25	1.57	1.47	1.57	1.54

transmission coefficients for tunneling. As expected, SCT is better for small to intermediate curvature and LCT is better for large curvature. The μOMT transmission coefficient also underestimates tunneling but is the best choice when the LAT transmission coefficient is considered to be too expensive.

For reaction R1, we compare the thermal rate constants with accurate multidimensional quantum dynamical calculations[68] in the interval 200−500 K. There are also previous CVT/μOMT calculations[69] for the same interval of temperatures, which showed very good agreement with the previous quantum calculations. The CVT/LAT rate constants obtained in this work show even better agreement with the quantum

Table 2. VTST/MT Thermal Rate Constants (in cm^3 $Molecule^{-1}$ s^{-1}) Compared to Accurate Quantal Ones for Reaction R1 on the JG Surface

T (K)	CVT/SCT[a]	CVT/LCT[a]	CVT/μOMT[a]	CVT/LAT[b]	accurate[c]
200	7.1(−21)[d]	5.2(−21)	7.1(−21)	1.0(−20)	9.0(−21)
250	4.3(−19)	3.5(−19)	4.3(−19)	5.0(−19)	5.5(−19)
300	7.8(−18)	6.7(−18)	7.8(−18)	8.2(−18)	9.8(−18)
400	3.6(−16)	3.3(−16)	3.6(−16)	3.6(−16)	4.0(−16)
500	4.1(−15)	3.8(−15)	4.1(−15)	4.0(−15)	3.8(−15)

[a] From ref 69. [b] This work. [c] From ref 68. [d] Powers of 10 in parentheses.

Table 3. Transmission Coefficients for Reaction R2 on the JG Surface

T (K)	ZCT	SCT	LCT	μOMT	LAT
200	2.98	4.62	31.3	31.3	36.5
250	2.08	2.83	11.3	11.3	12.5
300	1.69	2.12	6.14	6.14	6.59
400	1.35	1.56	3.10	3.10	3.23
500	1.22	1.34	2.16	2.16	2.22

results. The μOMT transmission coefficients are identical to the SCT ones, indicating that the least-action path is quite far from the straight path. Therefore, in this case the LCT transmission coefficients underestimate quantum effects. Sansón et al.[70] reached a similar conclusion for the $H_2 + Cl$ reaction, which has similar skew angle to reaction R1. Because the skew angle for R1 is not large (small-to-intermediate curvature case), it is expected that the SCT transmission coefficient accounts well for tunneling. However, the comparison between SCT and LAT at $T = 200$ K shows that SCT underestimates tunneling at this temperature, although the difference is already small at room temperature. From the comparison of CVT/SCT and CVT/LAT with the accurate rate constants, it is difficult to know which of the two transmission coefficients is more accurate because both approximations lead to very good results; LAT could be more accurate than SCT because it finds the optimum tunneling paths in a set of paths at every tunneling energy and it includes nonadiabaticity; but SCT could also be more accurate because it incorporates a more accurate treatment of systems in the small-curvature limit.

When the curvature of the reaction path is large, as for reaction R2, SCT seriously underestimates tunneling at all temperatures in the range 200−500 K (Table 3) and, therefore, this approximation accounts poorly for quantum effects in this case. The LAT transmission coefficients are also larger than the LCT ones. The straight path used in the LCT method is a particular path in the family of paths generated by eq 13, and the LCT calculation corresponds, at every energy for which $\tilde{\alpha}$ does not equal 1 to an incompletely optimized LAG calculation (whereas SCT does not). Thus, whenever LCT differs from LAT, it gives less transmission probability. However, the LAT transmission factor is underestimated by LCT by only 14% at $T = 200$ K, and this percentage is reduced by half at room temperature.

To further analyze the tunneling, we examined, at every temperature, the integrand of eq 5, $P_W(E)$, which is the Boltzmann-weighted transmission probability. The value of P_W, with the zero of energy taken here as the maximum of

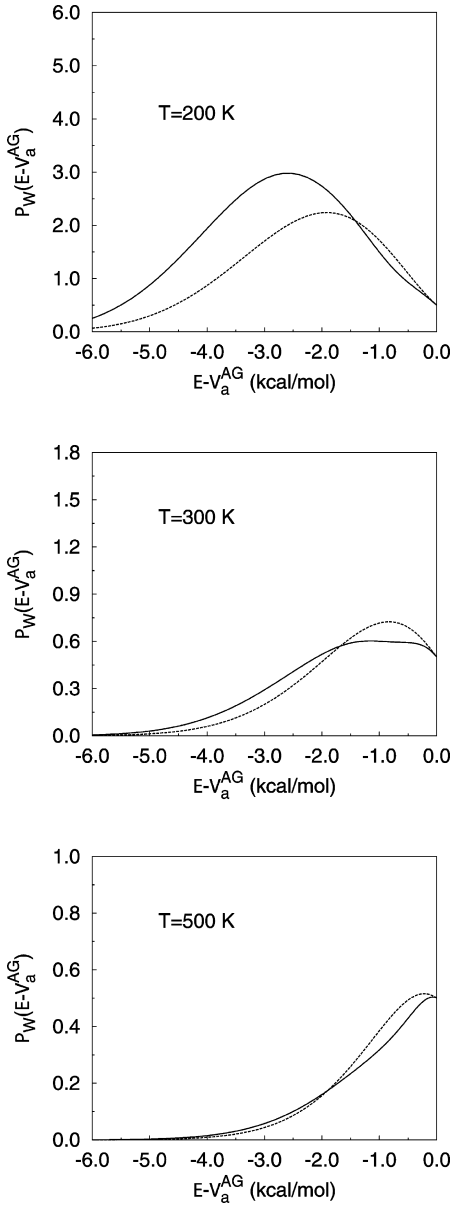

Figure 3. Representation of the LAT (solid line) and μOMT (dashed line) Boltzmann-weighted probabilities versus tunneling energy at different temperatures for reaction R1. The tunneling energies labeling the abscissa are calculated using the maximum of the vibrationally adiabatic ground-state potential curve, V_a^{AG}, as the temporary zero of energy.

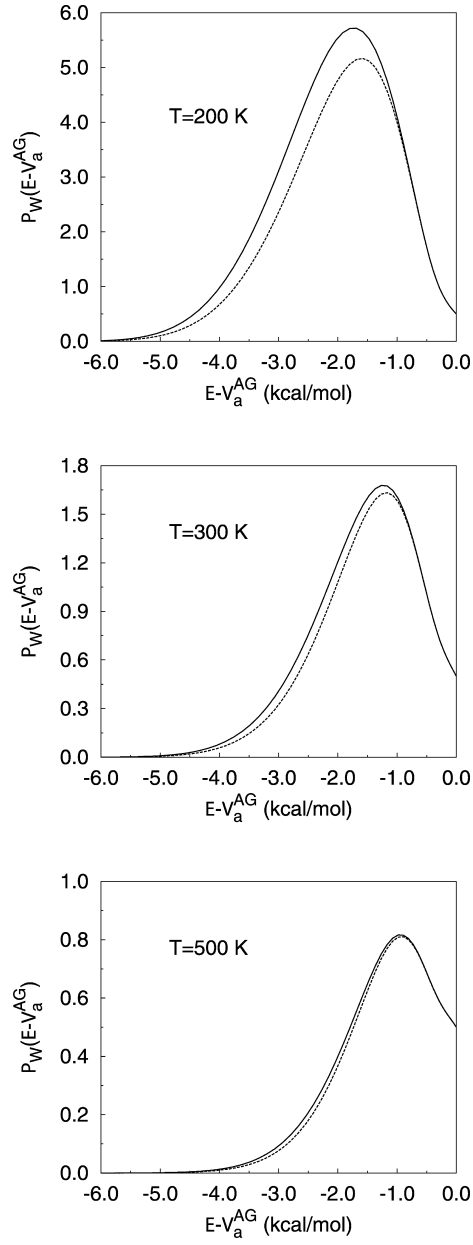

Figure 4. Same as Figure 3 but for reaction R2.

the vibrationally adiabatic ground-state potential curve, is shown at several temperatures for reactions R1 and R2 in Figures 3 and 4, respectively. The area under the curves gives the tunneling contribution to the transmission coefficients, which is clearly more important for reaction R2. Figures 3 and 4 also show how P_W varies with the tunneling energy for different transmission coefficients. Taking the LAT approximation as a reference approximation, we observe that for reaction R2 the μOMT curve follows closely the LAT curve, and as a consequence the μOMT transmission coefficients are quite similar to the LAT ones. For reaction R1, the μOMT transmission probabilities coincide with the SCT ones but that curve is quite far from the LAT curve at $T = 200$ K due to the difference in magnitude of the transmission coefficients. At $T = 300$ K and above the magnitude of SCT and LAT transmission coefficients is similar, and the curves are similar, but they differ in detail, with the μOMT (or SCT) probabilities being smaller at low tunneling energies, and bigger at high tunneling energies, when compared with the LAT probabilities. This behavior is observed even at $T = 200$ K and indicates that the SCT probabilities are too high at tunneling energies close to the top of the barrier. Another argument supporting this conclusion is offered during the discussion of the graphs depicted in Figure 5 and Figure 6.

The Boltzmann-weighted probability also allows one to identify the tunneling energy that contributes the most to each transmission coefficient. This characteristic energy is called representative tunneling energy (RTE), and it can be easily identified as the energy for which P_W has a maximum. The RTEs for reactions R1 and R2 obtained by each of the approximations for tunneling are listed in Tables 4 and 5, respectively. If the temperature is high, the maximum

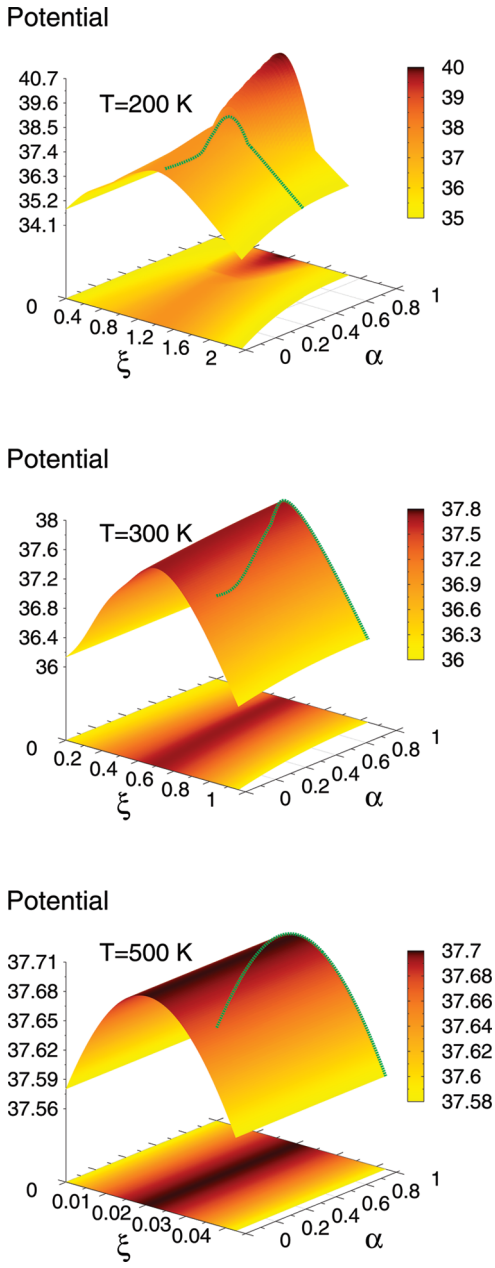

Figure 5. Effective potentials (in kcal/mol) at the representative tunneling energy for reaction R1 at different temperatures. The *X* axis is the length of the path, ξ (in a_0), and the *Y* axis is the α parameter (eq 13), which controls the curvature of the tunneling path. The green lines in each of the graphs are the least-action paths for that particular RTE. See text for details.

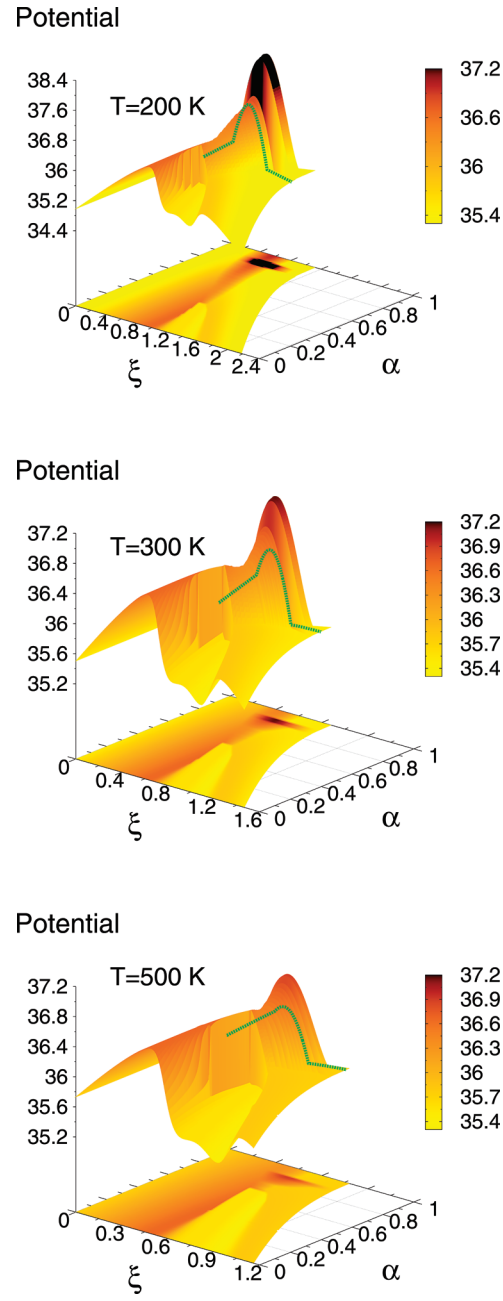

Figure 6. Same as Figure 5 but for reaction R2.

Table 4. Representative Tunneling Energies for Reaction R1 (in kcal mol^{-1})[a]

T (K)	ZCT	SCT	LCT	μOMT	LAT
200	37.03	35.68	36.07	35.68	34.75
250	37.29	36.42	36.14	36.42	36.11
300	37.42	36.81	36.18	36.81	36.16
400	37.61	37.21	37.46	37.21	37.45
500	37.70	37.39	37.59	37.39	37.58

[a] The maximum of the vibrationally adiabatic ground-state potential curve has an energy of 37.70 kcal mol^{-1}.

coincides with the top of the barrier, indicating that tunneling is unimportant. Whereas the LAT imaginary action integral and therefore the tunneling probability is the best compromise between length and energetics for the family of paths of eq 13, the RTE is the best compromise between the tunneling probability and the Boltzmann factor. It is obvious that at low temperatures the RTE is located at relatively low energies. In the limiting case, at $T = 0$ K the only contribution to the transmission coefficient comes from the tunneling probability at the lowest tunneling energy (i.e., the zero-point energy). As temperature increases, more energy levels are populated, and tunneling is possible at several energies, and in this case we have to look for the least-action path at every tunneling energy. A quite different approach, known as the *instanton* theory[71,72] seeks, at every temperature (not at every energy) for a unique least-action periodic trajectory, called *instanton*, that represents all trajectories.

Table 5. Representative Tunneling Energies for Reaction R1 (in kcal mol^{-1})[a]

T (K)	ZCT	SCT	LCT	μOMT	LAT
200	35.90	35.81	35.01	35.01	34.95
250	36.14	35.86	35.34	35.34	35.11
300	36.28	36.00	35.53	35.53	35.52
400	36.57	36.23	35.71	35.71	35.71
500	36.65	36.37	35.74	35.74	35.74

[a] The maximum of the vibrationally adiabatic ground-state potential curve has an energy of 36.66 kcal mol^{-1}.

Unfortunately, above a given critical temperature (usually for temperatures above 250 K) there is no *instanton* trajectory, although it is still possible to solve the problem approximately using analytical expressions.[73] There is a certain resemblance between RTE and *instanton* in the sense that, at every temperature, both indicate the most relevant region of the PES for tunneling.

Figures 5 and 6 depict effective potentials, which are given by eq 19 in the nonadiabatic region and by the vibrationally adiabatic ground-state potential in the adiabatic region, versus the length of the path for several values of α, taking as turning points the representative tunneling energies at $T =$ 200, 300, and 500 K for reactions R1 and R2, respectively. Each of the graphs was generated by mapping the PES using eq 13. The green lines depicted in each of the graphs represent the least-action path. At $T = 200$ K the least action paths for both reactions, R1 and R2, have nonadiabatic regions, and the value of $\tilde{\alpha}$ is 0.62 and 0.83, respectively. For reaction R1 the ratio $\xi_P(\tilde{\alpha})/\xi_P(0)$ is 0.78 and the difference $V_{max}(\tilde{\alpha}) - V_a^{AG}$ is 0.64 kcal mol^{-1}, whereas for reaction R2 the ratio between lengths is 0.53 and the difference in energy is only 0.05 kcal mol^{-1}. Those numbers show that at $T = 200$ K the shortcut through the nonadiabatic region compensates the rise in energy for both reactions. This behavior is more noticeable for reaction R2, which exhibits a larger reaction-path curvature.

From the previous discussion it seems odd that, at $T =$ 300 K, $\tilde{\alpha}$ is 1.00 and 0.93 for reactions R1 and R2 respectively but it is easily understood by taking into account that for the former reaction all members of the family of curves at that temperature from $\alpha = 0$ to $\alpha = 1$ lie completely in the adiabatic region, so the maximum of the effective potential is always the maximum of the vibrationally adiabatic ground-state potential, as shown in Figure 5. The consequence is that there is no energy penalty for shorter paths and, therefore, the least-action path coincides with the straight path. This circumstance does not occur for reaction R2, which has a nonadiabatic region for some values of α. Therefore, when the relevant part of the reaction swath is completely adiabatic the least-action path should be always the straight path and the probabilities obtained with the SCT approximation should not be larger than the LCT ones in that region of the PES. However this occurs for reaction R1, as shown previously in Figure 3. On the light of the values of the transmission coefficients obtained by the SCT and LAT approximations for R1 this issue seems unimportant, but in future work it would be interesting to analyze this behavior in more depth for a large number of reactive systems presenting varying amounts of reaction-path curvature.

In this work, we have used an analytical PES to show how the LAT approximation works for polyatomic systems. However, the method is very expensive in computer time, which is an obstacle for on-the-fly generation of the PES. The easiest solution to the problem is a brute-force approach consisting in the evaluation of several tunneling energies at the same time by parallelization of the method. A more reasonable approach would be to make use of different interpolation procedures to save computer time. The two graphs of Figure 2 give us a hint about a possible solution to the problem. In principle, it would be feasible to use a spline under tension similar to the one used in the ILCT2D[62] approximation, with the difference that, instead of interpolating tunneling paths and tunneling energies, we interpolate imaginary-action integrals and tunneling energies. It is possible to make the procedure even less expensive in computer time by interpolating the potential needed for the evaluation of the imaginary-action integral at every α value. A more detailed discussion about how to extend the LAT method to make it practical for its use within the direct dynamics approach will be presented elsewhere.

5. Concluding Remarks

We have extended the least-action tunneling (LAT) approximation to polyatomic reactions. The implementation is called least-action ground-state version 4 because it is based on the reactant ground state when the reaction is written in the exoergic or thermoneutral direction and because in the limit of large reaction-path curvature it reduces to the large-curvature tunneling (LCT) approximation carried out by the large-curvature ground-state version 4 (LCG4) method. The new method is more complete than the simpler microcanonically optimized multidimensional tunneling (μOMT) approximation, and in the tests presented here it is slightly more accurate. The method has been incorporated in the *POLYRATE* computer program.

Acknowledgment. A.F.-R. and R.M.-P. thank the Dirección Xeral de Promoción Científica e Tecnolóxica do SUG (Xunta de Galicia) for financial support through Project No.2006/AX128. This work was supported in part by the U.S. Department of Energy, Office of Basic Energy Sciences under grant no. DE-FG02-86ER13579.

References

(1) Gamow, G. *Z. Phys.* **1928**, *51*, 204.

(2) Eckart, C. *Phys. Rev.* **1930**, *35*, 1303.

(3) Johnston, H. S. *Gas Phase Reaction Rate Theory*; Ronald Press: New York, 1966.

(4) Wigner, E. *Z. Phys. Chem.* **1932**, *B19*, 203.

(5) Bell, R. *Proc. R. Soc. London, Ser. A* **1933**, *139*, 466.

(6) Garrett, B. C.; Truhlar, D. G. *J. Chem. Phys.* **1980**, *72*, 3460.

(7) Garrett, B. C.; Truhlar, D. G.; Bowman, J. M.; Wagner, A. F.; Robie, D.; Arepalli, S.; Presser, N.; Gordon, R. J. *J. Am. Chem. Soc.* **1986**, *108*, 3515.

(8) Alhambra, C.; Sanchez, M. L.; Corchado, J. C.; Gao, J.; Truhlar, D. G. *Chem. Phys. Lett.* **2002**, *355*, 388.

(9) Nagel, Z.; Klinman, J. P. *Chem. Rev.* **2006**, *106*, 3095.

(10) *Isotope Effects in Chemistry and Biology*; Kohen, A., Limbach, H. H., Eds.; CRC Press: Boca Raton, FL, 2006.

(11) *Hydrogen-Transfer Reactions*; Hynes, J. T., Klinman, J. P., Limbach, H. H., Schowen, R. L., Eds.; Wiley-VCH: Weinheim, Germany, 2007.

(12) Truhlar, D. G.; Isaacson, A. D.; Garrett, B. C. Generalized Transition State Theory. In *Theory of Chemical Reaction Dynamics*; Baer, M., Ed.; CRC Press: Boca Raton, FL, 1985; Vol. 4 pp 65−137.

(13) Fernández-Ramos, A.; Ellingson, B. A.; Garrett, B. C.; Truhlar, D. G. Variational Transition State Theory with Multidimensional Tunneling. In *Reviews in Computational Chemistry*; Lipkowitz, K. B., Cundari, T. R., Eds.; Wiley-VCH: Washington, D. C., 2007; Vol. 23 pp 125−232.

(14) Truhlar, D. G.; Gao, J.; Garcia-Viloca, M.; Alhambra, C.; Corchado, J.; Sanchez, M. L.; Poulsen, T. D. *Int. J. Quantum Chem.* **2004**, *100*, 1135.

(15) Pu, J.; Gao, J.; Truhlar, D. *Chem. Rev.* **2006**, *106*, 3140.

(16) Jordan, M.; Gilbert, R. *J. Chem. Phys.* **1995**, *102*, 5669.

(17) Wigner, E. *J. Chem. Phys.* **1937**, *5*, 720.

(18) Horiuti, J. *Bull. Chem. Soc. Jpn.* **1938**, *13*, 210.

(19) Keck, J. C. *Adv. Chem. Phys.* **1967**, *13*, 85.

(20) Garrett, B. C.; Truhlar, D. G. *J. Chem. Phys.* **1979**, *70*, 1593.

(21) Garrett, B. C.; Truhlar, D. G. *Acc. Chem. Res.* **1980**, *13*, 440.

(22) Pechukas, P. *Annu. Rev. Phys. Chem.* **1981**, *32*, 159.

(23) Truhlar, D. G.; Hase, W. L.; Hynes, J. T. *J. Phys. Chem.* **1983**, *87*, 2664.

(24) Truhlar, D. G.; Garrett, B. C. *Annu. Rev. Phys. Chem.* **1984**, *35*, 159.

(25) Truhlar, D. G.; Garrett, B. C. *Annu. Rev. Phys. Chem.* **1984**, *35*, 159.

(26) Truhlar, D. G.; Garrett, B. C.; Klippenstein, S. J. *J. Phys. Chem.* **1996**, *100*, 12771.

(27) Eyring, H. *J. Chem. Phys.* **1935**, *3*, 107.

(28) Evans, M. G.; Polanyi, M. *Trans. Faraday Soc.* **1935**, *31*, 875.

(29) Tucker, S. C.; Truhlar, D. G. *NATO ASI Ser. C* **1989**, *13*, 291.

(30) Hirschfelder, J. O.; Wigner, E. *J. Chem. Phys.* **1939**, *7*, 616.

(31) Truhlar, D. G.; Kupperman, A. *J. Am. Chem. Soc.* **1971**, *93*, 1840.

(32) Kuppermann, A. *J. Phys. Chem.* **1979**, *83*, 171.

(33) Garrett, B. C.; Truhlar, D. G.; Grev, R. S.; Magnuson, A. W. *J. Phys. Chem.* **1980**, *84*, 1730.

(34) Fukui, K.; Kato, S.; Fujimoto, H. *J. Am. Chem. Soc.* **1975**, *97*, 1.

(35) Garrett, B. C.; Truhlar, D. G. *J. Phys. Chem.* **1979**, *83*, 1052.

(36) Pollak, E.; Pechukas, P. *J. Am. Chem. Soc.* **1978**, *100*, 2984.

(37) Fernández-Ramos, A.; Ellingson, B. A.; Meana-Pañeda, R.; Marques, J.; Truhlar, D. G. *Theor. Chem. Acc.* **2007**, *118*, 813.

(38) Ellingson, B. A.; Lynch, B. A.; Mielke, S. L.; Truhlar, D. G. *J. Chem. Phys.* **2006**, *125*, 84305.

(39) Sturdy, Y. K.; Clary, D. C. *Phys. Chem. Chem. Phys.* **2007**, *9*, 2397.

(40) Truhlar, D. G.; Kuppermann, A. *J. Chem. Phys.* **1972**, *56*, 2232.

(41) Allison, T. C.; Truhlar, D. G. Testing the Accuracy of Practical Semiclassical Methods: Variational Transition State Theory with Optimized Multidimensional Tunneling. In *Modern Methods for Multidimensional Dynamics Computations in Chemistry*; World Scientific: Singapore, 1998; pp 618–712.

(42) Wyatt, R. E. *J. Chem. Phys.* **1969**, *51*, 3489.

(43) Marcus, R. A. *J. Chem. Phys.* **1966**, *45*, 4493.

(44) Marcus, R. A.; Coltrin, M. E. *J. Chem. Phys.* **1977**, *67*, 2609.

(45) Garrett, B. C.; Truhlar, D. G. *Proc. Natl. Acad. Sci. U.S.A.* **1979**, *76*, 4755.

(46) Skodje, R. T.; Truhlar, D. G.; Garrett, B. C. *J. Phys. Chem.* **1981**, *85*, 3019.

(47) Skodje, R. T.; Truhlar, D. G.; Garrett, B. C. *J. Chem. Phys.* **1982**, *77*, 5955.

(48) Lu, D.-h.; Truong, T. N.; Melissas, V. S.; Lynch, G. C.; Liu, Y.-P.; Garrett, B. C.; Steckler, R.; Isaacson, A. D.; Rai, S. N.; Hancock, G. C.; Lauderdale, J. G.; Joseph, T.; Truhlar, D. G. *Comput. Phys. Commun.* **1992**, *71*, 235.

(49) Liu, Y.-P.; Lynch, G. C.; Truong, T. N.; Lu, D.-h.; Truhlar, D. G. *J. Am. Chem. Soc.* **1993**, *115*, 2408.

(50) Babamov, V. K.; Marcus, R. A. *J. Chem. Phys.* **1978**, *74*, 1790.

(51) Garrett, B. C.; Truhlar, D. G.; Wagner, A. F.; Dunning Jr, T. H. *J. Chem. Phys.* **1983**, *78*, 4400.

(52) Garrett, B. C.; Abusalbi, N.; Kouri, D. J.; Truhlar, D. G. *J. Chem. Phys.* **1985**, *83*, 2252.

(53) Garrett, B. C.; Joseph, T.; Truong, T. N.; Truhlar, D. G. *Chem. Phys.* **1989**, *136*, 271.

(54) Truong, T. N.; Lu, D.-h.; Lynch, G. C.; Liu, Y.-P.; Melissas, V. S.; Stewart, J. J. P.; Steckler, R.; Garrett, B. C.; Isaacson, A. D.; González-Lafont, A.; Rai, S. N.; Hancock, G. C.; Joseph, T.; Truhlar, D. G. *Comput. Phys. Commun.* **1993**, *75*, 143.

(55) Liu, Y.-P.; Lu, D.-h.; González-Lafont, A.; Truhlar, D. G.; Garrett, B. C. *J. Am. Chem. Soc.* **1993**, *115*, 7806.

(56) Fernández-Ramos, A.; Truhlar, D. G. *J. Chem. Phys.* **2001**, *114*, 1491.

(57) Miller, W. H.; Ruf, B. A.; Chang, Y. T. *J. Chem. Phys.* **1988**, *89*, 6298.

(58) Ruf, B. A.; Miller, W. H. *J. Chem. Soc., Faraday Trans. 2* **1988**, *84*, 1523.

(59) Makri, N.; Miller, W. H. *J. Chem. Phys.* **1989**, *91*, 4026.

(60) Kreevoy, M. M.; Ostovic, D.; Truhlar, D. G.; Garrett, B. C. *J. Phys. Chem.* **1986**, *90*, 3766.

(61) Fernández-Ramos, A.; Truhlar, D. G.; Corchado, J.; Espinosa-Garcia, J. *J. Phys. Chem. A* **2002**, *106*, 4957.

(62) Fernández-Ramos, A.; Truhlar, D. G. *J. Chem. Theory Comput.* **2005**, *1*, 1063.

(63) Garrett, B. C.; Truhlar, D. G. *J. Chem. Phys.* **1983**, *79*, 4931.

(64) Lynch, G. C.; Truhlar, D. G.; Garrett, B. C. *J. Chem. Phys.* **1989**, *90*, 3102.

(65) Taketsugu, T.; Kimihiko, H. *J. Chem. Phys.* **1997**, *107*, 10506.

(66) (a) Tautermann, C. S.; Voegele, A. F.; Loerting, T.; Liedl, K. R. *J. Chem. Phys.* **2002**, *117*, 1962. (b) Tautermann, C. S.; Voegele, A. F.; Loerting, T.; Liedl, K. R. *J. Chem. Phys.* **2002**, *117*, 1967. (c) Tautermann, C. S.; Voegele, A. F.; Liedl, K. R. *J. Chem. Phys.* **2004**, *120*, 631.

(67) Zheng, J.; Zhang, S.; Lynch, B. J.; Corchado, J. C.; Chuang, Y.-Y.; Fast, P. L.; Hu, W.-P.; Liu, Y.-P.; Lynch, G. C.; Nguyen, K. A.; Jackels, C. F.; Fernández Ramos, A.; Ellingson, B. A.; Melissas, V. S.; Villa, J.; Rossi, I.; Coitiño, E. L.; Pu, J.; Albu, T. V.; Steckler, R.; Garrett, B. C.; Isaacson, A. D.; Truhlar, D. G. *POLYRATE 2008*; University of Minnesota: Minneapolis, 2008.

(68) (a) Bowman, J. M.; Wang, D.; Huang, X.; Huarte-Larrañaga, F.; Manthe, U. *J. Chem. Phys.* **2001**, *114*, 9683. (b) Huarte-Larrañaga, F.; Manthe, U. *J. Chem. Phys.* **2002**, *116*, 2863.

(69) (a) Pu, J. C.; Corchado, J.; Truhlar, D. G. *J. Chem. Phys.* **2001**, *115*, 6266. (b) Pu, J.; Truhlar, D. G. *J. Chem. Phys.* **2002**, *117*, 1479.

(70) Sansón, J. A.; Sánchez, M. L.; Corchado, J. *J. Phys. Chem. A* **2005**, *110*, 589.

(71) (a) Miller, W. H. *J. Chem. Phys.* **1975**, *62*, 1899. (b) Coleman, S. *Phys. Rev. D* **1977**, *15*, 2929. (c) Benderskii, V.; Makarov, D. E.; Wight, C. H. *Adv. Chem. Phys.* **1994**, *88*, 1.

(72) Zhao, Y.; Yamamoto, T.; Miller, W. H. *J. Chem. Phys.* **2004**, *120*, 3100.

(73) Fernández-Ramos, A.; Smedarchina, Z.; Siebrand, W.; Zgierski, M. Z.; Rios, M. A. *J. Am. Chem. Soc.* **1999**, *121*, 6280.

CT900420E